Tight Coupling Between Electrical Activity and Exocytosis in Mouse Glucagon-Secreting α-Cells

Sebastian Barg, Juris Galvanovskis, Sven O. Göpel, Patrik Rorsman, and Lena Eliasson

α-Cells were identified in preparations of dispersed mouse islets by immunofluorescence microscopy. A high fraction of α-cells correlated with a small cell size measured as the average cell diameter (10 μm) and whole-cell capacitance (<4 pF). The α-cells generated action potentials at a low frequency (1 Hz) in the absence of glucose. These action potentials were reversibly inhibited by elevation of the glucose concentration to 20 mmol/l. The action potentials originated from a membrane potential more negative than –50 mV, had a maximal upstroke velocity of 5 V/s, and peaked at +1 mV. Voltage-clamp experiments revealed the ionic conductances underlying the generation of action potentials. α-Cells are equipped with a delayed tetraethyl-ammonium–blockable outward current (activating at voltages above –20 mV), a large tetrodotoxin-sensitive Na^+ current (above –30 mV; peak current 200 pA at +10 mV), and a small Ca^{2+} current (above –50 mV; peak current 30 pA at +10 mV). The latter flowed through ω-conotoxin GVIA (25%)- and nifedipine-sensitive (50%) Ca^{2+}-channels. Mouse α-cells contained, on average, 7,300 granules, which undergo Ca^{2+}-induced exocytosis when the α-cell is depolarized. Three functional subsets of granules were identified, and the size of the immediately releasable pool was estimated as 80 granules, or 1% of the total granule number. The maximal rate of exocytosis (1.5 pF/s) was observed 21 ms after the onset of the voltage-clamp depolarization, which is precisely the duration of Ca^{2+}-influx during an action potential. Our results suggest that the secretory machinery of the α-cell is optimized for maximal efficiency in the use of Ca^{2+} for exocytosis. *Diabetes* 49:1500–1510, 2000

Glucagon is a major catabolic and hyperglycemic hormone of 29 amino acids and is secreted from the α-cells of the islets of Langerhans (1). Its main biological effect is the regulation of glucose metabolism by enhancing synthesis and mobilization of glucose in the liver. Normally, secretion of the hormone is stimulated by low blood glucose (2), amino acids (3), and a variety of hormones and neurotransmitters, such as adrenaline, glucose-dependent insulinotropic polypeptide, and glucagon-like peptide-1 (4,5). Hyperglycemia and fatty acids are the main inhibitors (6), but the islet hormones insulin and somatostatin (4) also appear to reduce glucagon secretion, possibly by a paracrine mechanism (7). Whereas insulin levels are inadequately low in hyperglycemic diabetic subjects, glucagon levels are actually elevated, and this increase exacerbates the disease (8). The reason for this abnormality is unknown, and studies on α-cells are complicated by the scarcity of islet tissue and the low occurrence of α-cells compared with β-cells. Therefore, how glucose physiologically regulates secretion in the α-cell remains unknown. Electrical activity in glucagon-secreting cells has been observed using several experimental approaches (5,9,10), and it is, at least in part, attributable to voltage-gated Ca^{2+} channels. Available evidence also suggests that glucagon release is a Ca^{2+}-dependent process. Indeed, capacitance measurements on single rat α-cells revealed a close relationship between N-type Ca^{2+} channels and the secretory granules under basal conditions, whereas L-type Ca^{2+} channels appeared more important when secretion was stimulated with adrenaline (5). The finding that glucagon secretion is Ca^{2+}-dependent, coupled with the fact that glucagon release is suppressed by glucose, suggests that the α-cells must be electrically silent at elevated glucose concentrations, contrary to the situation in the β-cell. Thus, it is surprising that ATP-sensitive potassium channels (i.e., channels that are inhibited by an increase in the intracellular ATP concentration [K_{ATP} channels]) have recently been documented in rat α-cells (11). So far, no data about the electrophysiology of mouse α-cells are available. However, experiments on α-cells in intact mouse islets (12), as well as isolated α-cells identified by immunocytochemistry (13), have provided evidence for Ca^{2+} oscillations at low glucose levels. These are often, but not always, suppressed by an elevation of the extracellular glucose concentration.

Here we report that it is possible to identify α-cells in preparations of dispersed mouse islets. This enables us to characterize the electrophysiological and exocytotic properties of individual mouse α-cells. We demonstrate that these cells can readily be distinguished from the β-cells by electrophysiological means. They are electrically active at low glucose levels and have lower cell capacitance (3–5 pF), a prominent tetrodotoxin (TTX)-sensitive Na^+ current, and 2 types of Ca^{2+} channels.

RESEARCH DESIGN AND METHODS

Cells. NMRI mice were purchased from a commercial breeder (Bomholtgaard, Ry, Denmark). The animals were anesthesized by pentobarbital (4 mg/animal i.p.) and subsequently killed by cervical dislocation. Pancreatic islets were isolated by collagenase P (16 U/ml, Boehringer Mannheim) digestion. Islets thus obtained were dissociated into single cells by shaking at low

From the Department of Molecular and Cellular Physiology, Diabetes Research Unit, Institute of Physiological Sciences, University of Lund, Lund, Sweden.

Address correspondence and reprint requests to Lena Eliasson, PhD, Department of Molecular and Cellular Physiology, Sölvegatan 19, SE-223 62 Lund, Sweden. E-mail: lena.eliasson@mphy.lu.se.

Received for publication 3 December 1999 and accepted in revised form 18 May 2000.

$[Ca^{2+}]_i$, intracellular Ca^{2+} concentration; IRP, immediately releasable pool; K_{ATP} channel, ATP-sensitive potassium channel; RRP, readily releasable pool; TEA, tetraethyl-ammonium; TTX, tetrodotoxin.

extracellular Ca^{2+} levels (14). The resultant cell suspension was plated on plastic petri dishes, and cells were maintained in tissue culture for up to 3 days in RPMI-1640 supplemented with 10% fetal calf serum, 100 U/ml penicillin, and 10 µg/ml streptomycin.

Immunohistochemistry. Islet cells were cultured for 4–28 h, fixed in 4% formaldehyde (Polyscience, Warrington, PA) in phosphate-buffered saline, and permeabilized with 0.1% Triton X100 for 20 min. After blocking of nonspecific sites with 5% normal donkey serum for 30 min, the cells were incubated for 1 h at 4°C with a 1:500–1,000 dilution of the primary antibodies (guinea pig anti-insulin, rabbit anti-glucagon [Eurodiagnostica, Sweden], and sheep anti-somatostatin [Biogenesis, Poole, U.K.]). Dye-conjugated (Cy2, Texas Red, and Cy5) donkey-raised secondary antibodies (Jackson Immuno) were used to label the detected sites. Immunofluorescence was visualized with a Zeiss LSM510 confocal microscope using a 20× objective (Carl Zeiss, Jena, Germany). The samples were scanned sequentially with the appropriate settings for each label to minimize crosstalk. Cells not stained at all were rarely observed (<0.5%) and may have been polypeptide-producing cells.

Electrophysiology. Membrane potential and whole-cell currents were recorded using EPC-9 patch-clamp amplifiers and the software Pulse (Heka Elektronik, Lamprecht/Pfalz, Germany). Exocytosis was detected as changes in cell capacitance using the software lock-in (which adds a 500 Hz sine wave to the holding potential) or the "captrack" function of the amplifier. Exocytosis was elicited either by infusion of a Ca^{2+}/EGTA-buffer with an intracellular Ca^{2+} concentration ($[Ca^{2+}]_i$) of 0 or 1.5 µmol/l through the recording electrode or by voltage-clamp depolarizations. Patch electrodes were pulled from borosilicate glass capillaries, coated with Sylgard, and fire-polished. The pipette resistance ranged between 3 and 6 MΩ when the pipettes were filled with intracellular solutions. Experiments were conducted using either the standard or the perforated patch whole-cell configuration as indicated. α-Cells were identified by a discernable Na^+ current and a C_m <4 pF and/or by their electrical activity in the absence of glucose that could be suppressed by the addition of glucose (10–20 mmol/l). Except for Fig. 1, only experiments from preparations containing at least 40% α-cells were included in the analysis. δ-Cells in excess of 2% were found in 1 of 13 preparations, and this preparation contained no α-cells.

Solutions. For the measurements of membrane potential, K^+ conductances, and the infusion experiments, the standard extracellular solution consisted of (in millimoles per liter) 138 NaCl, 5.6 KCl, 2.6 $CaCl_2$, 1.2 $MgCl_2$, and 5 HEPES (pH 7.4 using NaOH). In all other experiments, 20 mmol/l tetraethyl-ammonium (TEA) chloride (NaCl concentration reduced correspondingly to maintain osmolarity) was added to block voltage-gated K^+ currents. Except for the measurements of membrane potential (Fig. 2), in which the glucose concentration varied between 0–20 mmol/l (as indicated), the concentration of glucose was 5 mmol/l. For characterization of the Ca^{2+} current, extracellular $CaCl_2$ was replaced with 10 mmol/l $BaCl_2$. In results presented in Figs. 3 and 4, 0.1 mg/ml TTX was added to block the voltage-gated Na^+ currents. The

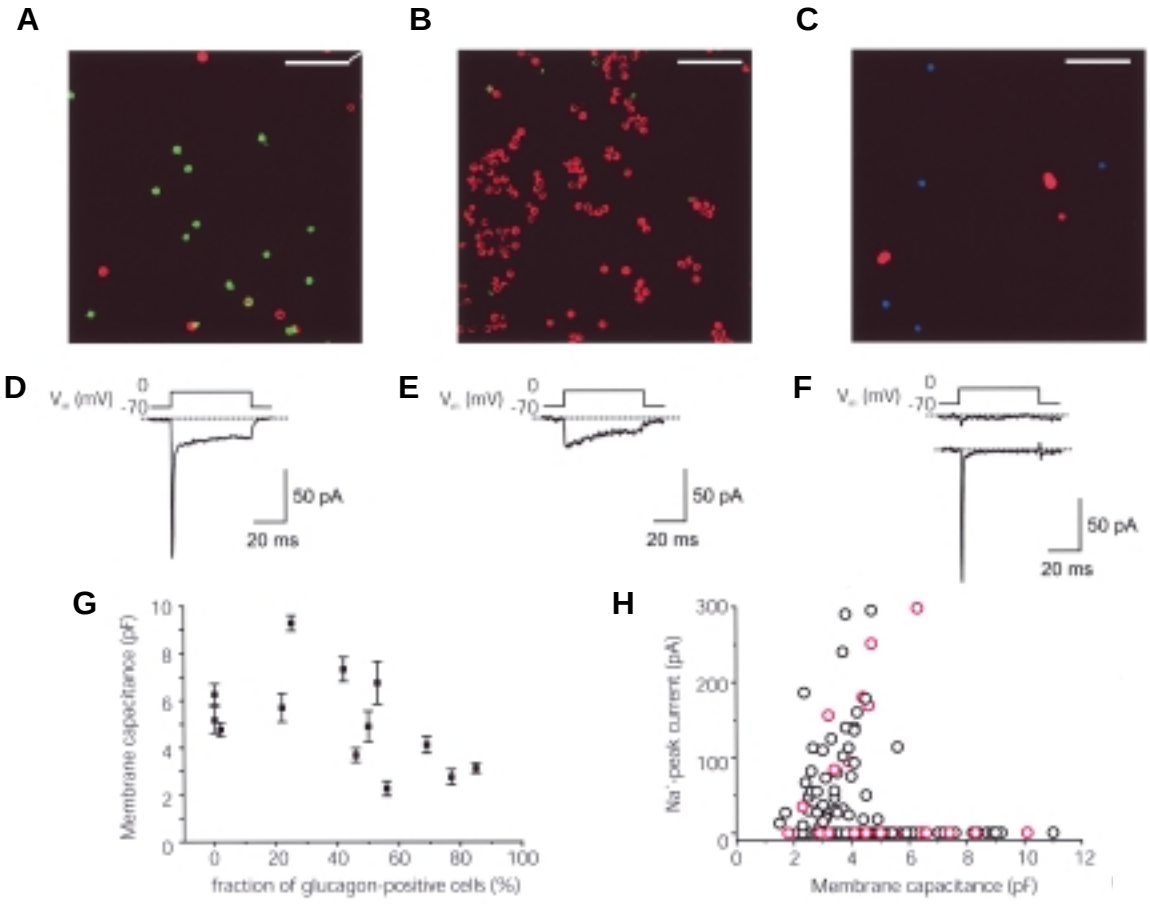

FIG. 1. High prevalence of glucagon-positive cells correlates with small cell size. *A–C*: Immunofluorescence micrographs of typical preparations of dispersed mouse islet cells. α-Cells are shaded green; β-cells are shaded red. The scale bar is 100 µm. The percentage of α- and β-cells in panel *A* was 69 and 31%, respectively. No δ-cells were seen. In panel *B*, the α- and β-cells constituted 2 and 98% of the total cell number. Again, no δ-cells were observed. The relative frequency of β- and δ-cells in panel *C* was 30 and 70%, respectively. No α-cells were seen in this preparation. *D*: Representative inward current response evoked by a 50-ms membrane depolarization from –70 to 0 mV in an α-cell–rich fraction. Note that the current response consists of an initial transient and a late sustained component. *E*: Representative inward current response evoked by a 50-ms membrane depolarization from –70 to 0 mV in a β-cell–rich fraction. Note the absence of the initial transient component. *F*: Currents recorded from non–β-cells in a δ-cell–rich preparation. In 27% of the cells, an inactivating current was observed. *G*: Average cell capacitance plotted against the percentage of α-cells for 13 individual preparations. *H*: The peak Na^+ current evoked by membrane depolarization from –70 to 0 mV plotted against cell capacitance. The experiments from the preparation shown in *C* are represented in red. Note that the Na^+ current is absent from cells with values for the cell capacitance >6 pF.

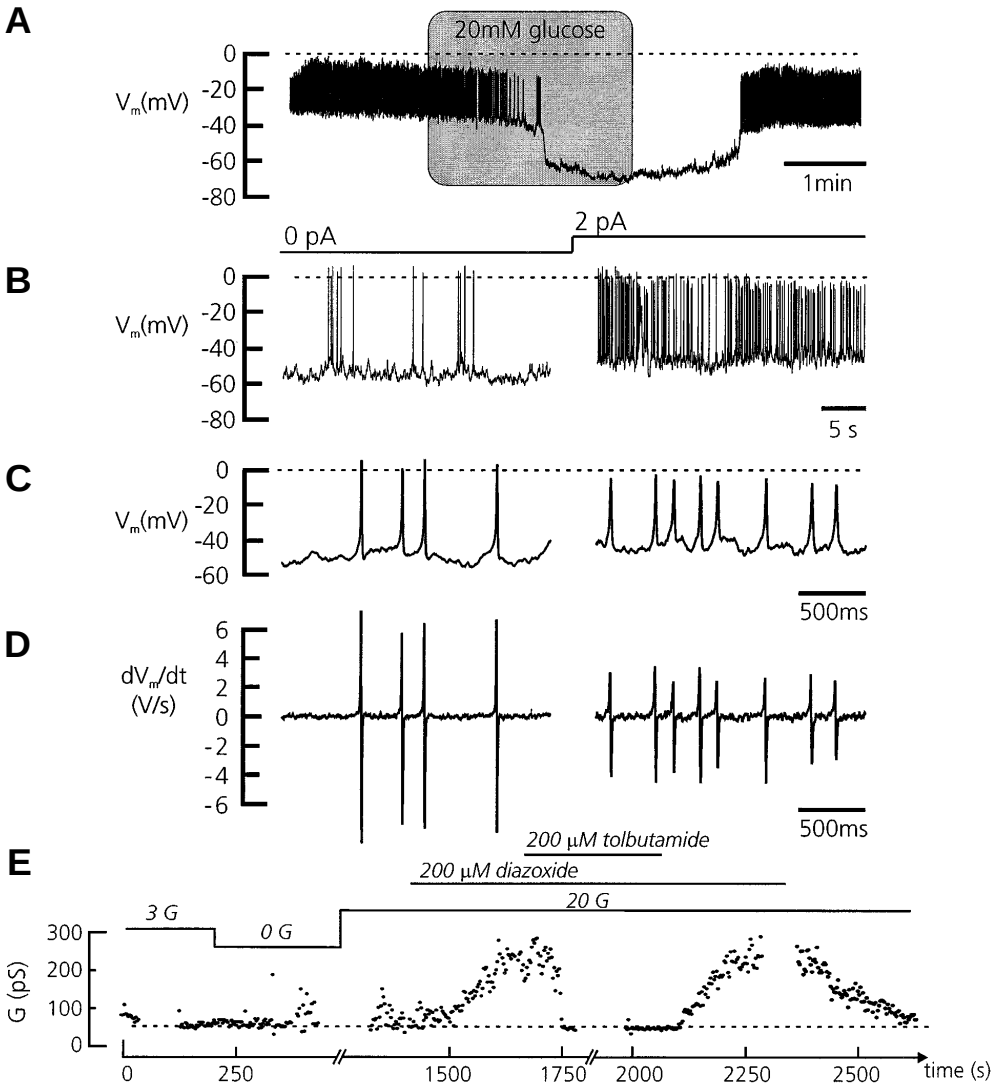

FIG. 2. Membrane potential and K_{ATP} conductance. *A*: Recordings of electrical activity from a single mouse pancreatic α-cell in the presence of 3 mmol/l glucose. Electrical activity ceased when the glucose concentration was increased to 20 mmol/l. *B*: Recordings of spontaneous action potentials. The spike frequency was increased by injection of 2 pA depolarizing current (by staircase above the voltage trace). *C*: Action potentials from panel *B* displayed using expanded vertical and horizontal scales. *D*: The derivative (*dV/dt*) of the α-cell action potentials in panel *C*. *E*: Whole-cell K^+ conductance estimated from ± 20 mV voltage excursion from the holding potential (–70 mV) in a single α-cell at different glucose concentrations, after addition of diazoxide (200 μmol/l) and tolbutamide (200 μmol/l) to the extracellular medium. Recordings were filtered at 0.2 kHz and digitized at 0.5 kHz.

pipette solution for recording Ca^{2+} currents consisted of (in millimoles per liter) 125 CsCl, 1 $MgCl_2$, 10 EGTA, 3 Mg-ATP, 10 HEPES (pH 7.15 using CsOH), and 0.1 cAMP. For studies of depolarization-evoked exocytosis, EGTA was reduced to 50 μmol/l, whereas an intracellular solution containing (in millimoles per liter) 125 K-glutamate, 10 KCl, 10 NaCl, 1 $MgCl_2$, 3 Mg-ATP, 0.1 cAMP, 10 HEPES, 10 EGTA, and 0 or 9 $CaCl_2$ was used in the Ca^{2+} infusion experiments. $[Ca^{2+}]_i$ in the latter medium was estimated to be <10 nmol/l and 1.5 μmol/l, respectively (15). For measurements of the whole-cell K^+ conductance, the pipette solution consisted of (in millimoles per liter) 120 KCl, 1 $MgCl_2$, 10 EGTA, 10 HEPES (pH 7.15), and 0.3 or 5 Mg-ATP. In the perforated patch experiments, the pipette solution contained (in millimoles per liter) 76 K_2SO_4, 10 KCl, 10 NaCl, 1 $MgCl_2$, 5 HEPES (pH 7.15 with KOH) and amphotericin B (added at a final concentration of 0.24 mg/ml to establish electrical contact) (16).

Electron microscopy. Pancreatic islets were incubated for 10–15 min in standard extracellular solution before fixation in 2.5% glutaraldehyde for 1 h. The islets were finally treated with 1% osmium tetroxide, dehydrated, and embedded in Epon 812 before being cut into ~60–80 nm ultrathin sections using an LKB MK III Ultratome. The sections were contrasted with uranyl citrate and examined in a Philips CM 10 electron microscope.

Data analysis. Unless otherwise indicated, the membrane currents were filtered at 3.3 kHz and digitized at 10 kHz. Leak currents and capacitive transients were removed using a –p/4 paradigm. Depolarization-evoked exocytotic responses are expressed as the net change in whole-cell capacitance (ΔC_m). For the current-clamp measurements, the membrane potential was filtered at 0.2 kHz and digitized at 0.5 kHz. In the infusion experiments, the linear increase during the first 60 s after the establishment of the whole-cell configuration was calculated.

The Ca^{2+} current during an action potential is described by the equation

$$I_{Ca} = g_{Ca} \cdot m \cdot (V_m - V_{Ca}) \quad (1)$$

where V_m is the variable action potential, V_{Ca} is the equilibrium potential for Ca^{2+}, g_{Ca} is the maximal conductance of the Ca^{2+} channel, and m is the activation variable, which satisfies a differential equation

$$\frac{dm}{dt} = \frac{m_\infty - m}{\tau_m} \quad (2)$$

with m_∞ defined as

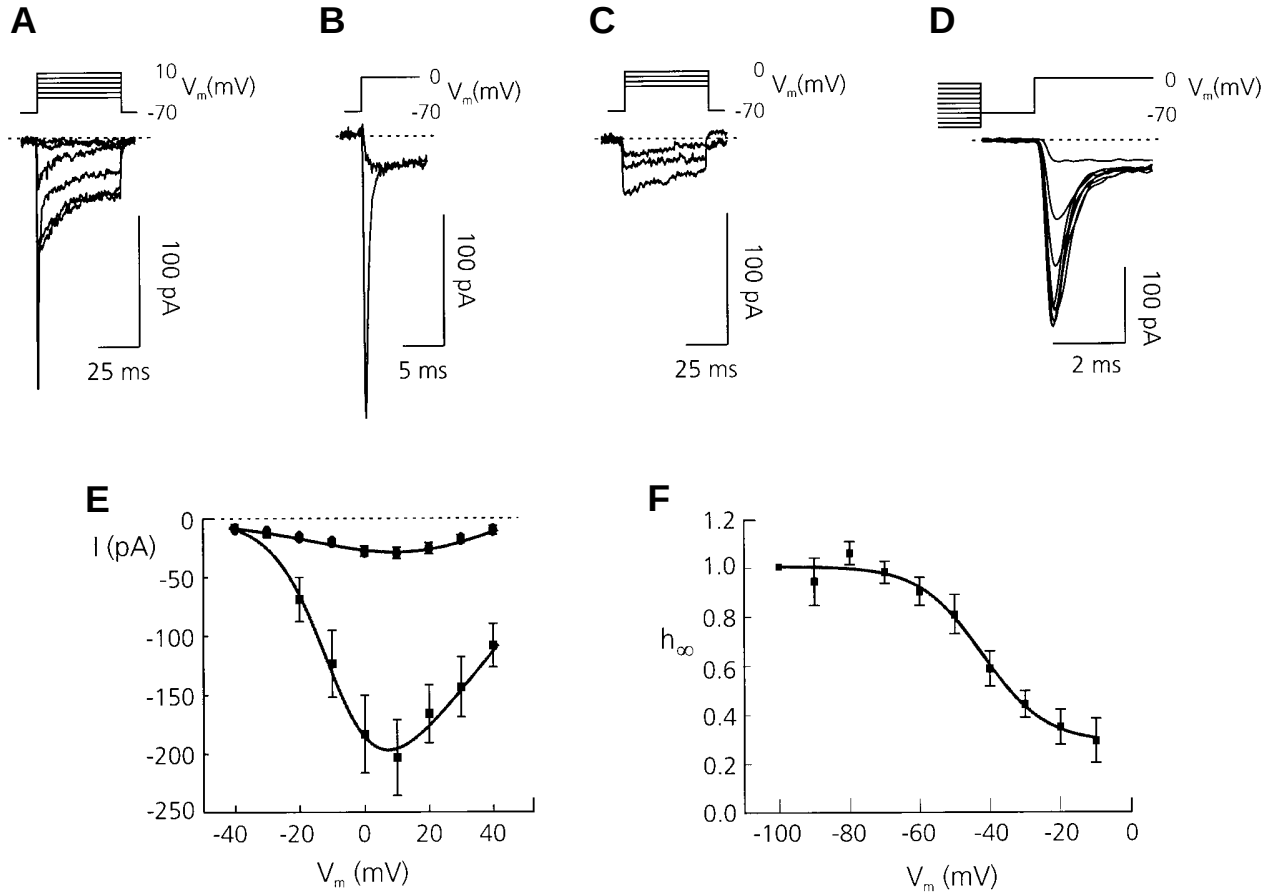

FIG. 3. Voltage-dependent and TTX-sensitive Na^+ currents in α-cells. *A*: α-Cells were depolarized for 50 ms from –70 mV to voltages between –40 and +40 mV in 10-mV increments. For clarity, only the responses between –40 mV and +10 are shown. *B*: The large inward current transient was blocked by inclusion of TTX (0.1 µg/ml). *C*: A family of inward currents recorded in the presence of TTX when the membrane potential was stepped between –20 and zero. *D*: The peak current *I-V* relationship in the absence (■) and presence (●) of TTX. The curve is drawn according to Eq. 4. *E*: Steady-state inactivation of the Na^+ current. Conditioning pulses of 50 ms (–100 to –10 mV) preceded the depolarization to 0 mV. Records were filtered at 10 kHz and digitized at 30 kHz. *F*: Relative current amplitude ($h_\infty = I/I_{max}$) plotted against the voltage during the conditioning pulse (V_m). The curve is drawn according to Eq. 5. Data are the means ± SE of 8 experiments.

$$m_\infty = \frac{1}{1 + e^{\frac{(V_h - V_m)}{k}}} \quad (3)$$

and τ_m being the time-constant of the Ca^{2+} current activation. V_h is the voltage at which the Ca^{2+} current is half-maximal, and k is the slope coefficient. Because we were interested only in the temporal relationship between the action potential and the current, the conductance g_{Ca} was set to 1 to get a unitary measure of the Ca^{2+} current.

The size of the immediately releasable pool (IRP) was determined by fitting Eq. 9 to the observed data points. The differential equations (Eq. 3 and Eq. 6) were solved numerically in Matlab (MathWorks, Natick, MA) with a Runge-Kutta 4th-order formula. The solution to Eq. 6 was then fit to experimental data using the Nelder-Mead simplex method.

Measurements of granule size in α-cells were performed on digitally scanned electron micrographs of thin sections of mouse pancreatic islets. The apparent diameter of individual granules was determined with the image-processing software 3D for LSM (Carl Zeiss, Jena, Germany). The actual diameter was then calculated using the method of Giger and Riedwyl (17). The density of granules in α-cells was estimated according to the procedures described by DeHoff and Rhines (18) and multiplied by the average cell volume as determined from the measured cell diameter (assuming spherical geometry) (19) to derive the total granule number. The linear size of a single pixel in figures was calculated on the basis of magnifications used in the preparation of the original electron micrographs.

Data are presented as means ± SE of indicated experiments (n). Statistical significance was assessed using Student's t test.

RESULTS

α-Cells can be identified by cell size. Immunofluorescence microscopy was used to estimate the relative frequency of α-cells in preparations of dispersed mouse pancreatic islet cells. Fig. 1*A–C* shows 3 examples that illustrate the variation of the ratio between glucagon- (green), insulin- (red), and somatostatin-positive cells (blue) in different preparations. Relative amounts of α-cells ranged from 0 to 85%. The frequency of δ-cells was <2%, except in a single preparation that contained 70% δ-cells, 30% β-cells, and no α-cells (Fig. 1*C*).

Inward currents evoked by a 50-ms depolarization (–70 to 0 mV) typical to the respective preparation are shown in Fig. 1*D–F*. In addition to the observed sustained Ca^{2+} current, cells in the α-cell preparation also contained a large Na^+ current. In the preparation rich in δ-cells (Fig. 1*C*), current responses in 27% of the cells were those expected for β-cells (Fig. 1*E*). In the remaining cells, depolarization evoked a large Na^+ current in 8 of 22 cells (Fig. 1*F*, lower panel), whereas current responses were small in the remaining 47% of the cells (Fig. 1*F*, upper panel). The cell capacitance of the cells with non–β-cell behavior in the latter preparation was 4.2 ± 0.3 pF (n = 22).

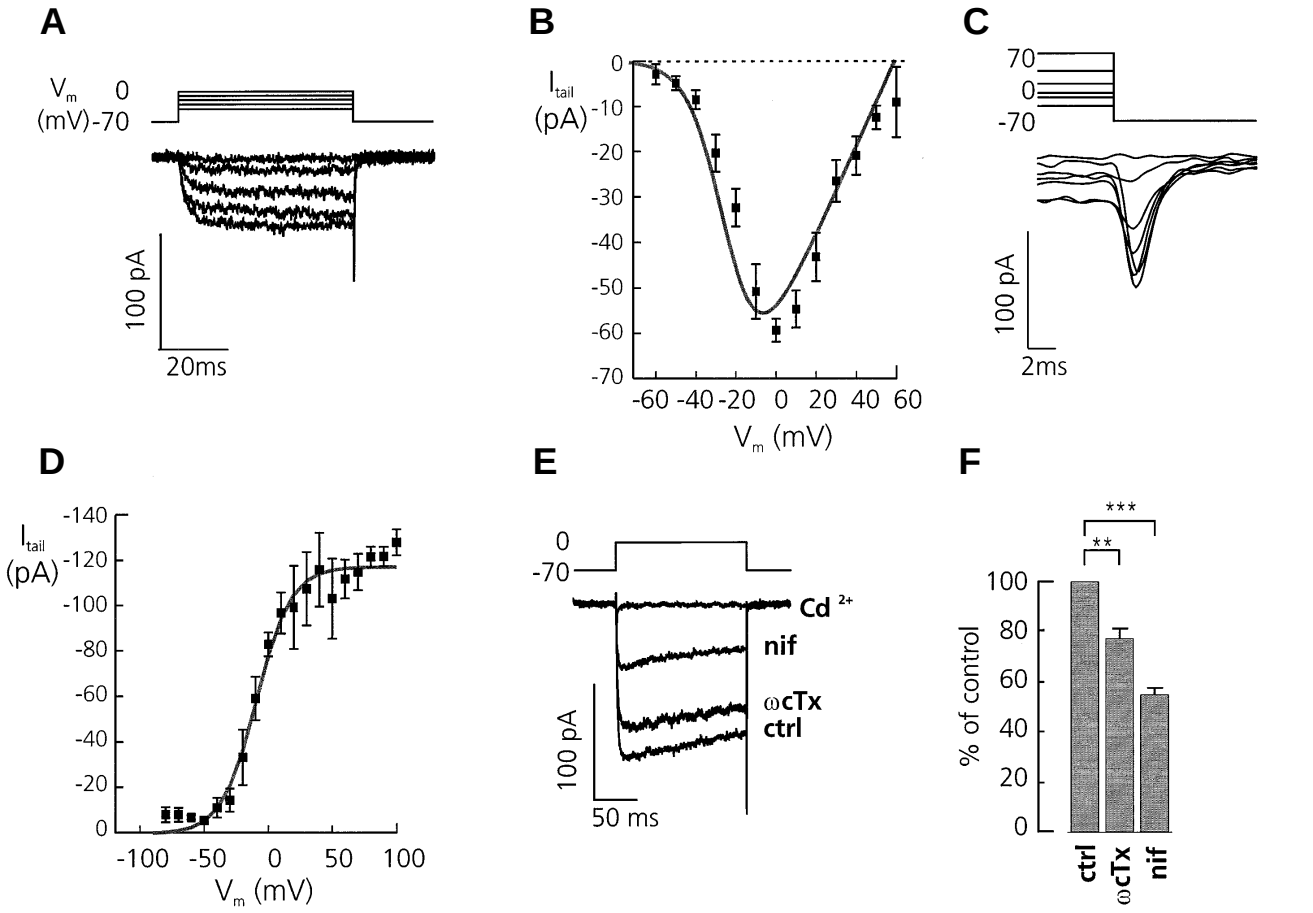

FIG. 4. Ca^{2+} currents in pancreatic α-cells. *A*: Ca^{2+} currents recorded with 10 mmol/l Ba^{2+} as the charge carrier. The cell was voltage-clamped at –70 mV and depolarized to voltages between –50 and 0 mV for 50 ms, as indicated schematically above the current traces. *B*: The *I-V* relationship for the Ca^{2+} channel current recorded in the presence of 10 mmol/l Ba^{2+} as the charge carrier. The curve is drawn according to Eq. 4. *C*: Tail currents recorded upon stepping to –70 mV after test pulses between –30 and +50 mV. *D*: Ca^{2+} current activation determined from the peak tail-current amplitude. The curve is drawn according to Eq. 5. *E*: Pharmacology of the Ca^{2+} current. The α-cell was clamped at –70 mV and depolarized to 0 mV for 200 ms. The Ca^{2+} channel blockers ω-conotoxin, nifedipine, and Cd^{2+} were added at concentrations of 1, 25, and 200 μmol/l, respectively. *F*: Effects of Ca^{2+} channel inhibitors on the normalized mean currents. ***P* < 0.01; ****P* < 0.001. nif, Nifedipine; ωcTx, ω-conotoxin.

Identification of α-cells by immunostaining before the electrophysiological experiments is not possible because it necessitates fixation and permeabilization. Instead, we correlated the fraction of α-cells in individual preparations to the average cell capacitance (Fig. 1*G*). We found average whole-cell capacitances of <4 pF only in preparations with a large fraction of α-cells (3.3 ± 0.2 pF, n = 28 cells) and of >5 pF in which the β-cell predominated (6.1 ± 0.3 pF, n = 67 cells). The cell diameter determined by confocal microscopy in α-, β-, and δ-cells could be described by Gaussians with midpoints of 10.6 μm (width at 50% height = 3.1 μm, n = 54), 14.8 μm (width = 3.2 μm, n = 63), and 11.8 μm (width = 1.9 μm, n = 38), respectively. Assuming spherical geometry and a specific capacitance of 10 fF/μm^2, these values translate to cell capacitances of 3.5, 6.9, and 4.4 pF for the α-, β-, and δ-cells, which are in reasonable agreement with the mean capacitance values obtained experimentally. The occurrence of transient Na^+ currents correlated well with the small cells (Fig. 1*H*), indicating that these cells are indeed α-cells. In typical preparations containing low amounts of δ-cells, it is therefore safe to identify α-cells based on their electrophysiological properties.

Glucose inhibits electrical activity in mouse α-cells. We proceeded by studying the membrane potential of the small cells in preparations with a high prevalence of α-cells. Regenerative action potentials could be observed at low glucose concentrations (0 or 3 mmol/l). The frequency of the spontaneous action potentials was low (1.0 ± 0.2 Hz, n = 5) but could be dramatically increased by the injection of small depolarizing currents. For example, injection of 2 pA current increased the action potential frequency 4-fold (Fig. 2*B* and *C*) to 4.0 ± 0.7 Hz (n = 4). The spontaneous action potentials originated at –52 ± 2 mV (n = 5) and peaked at 1 ± 4 mV (n = 5). The duration of the spontaneous action potentials averaged 31 ± 4 ms, and the rates of depolarization and repolarization were 4.9 ± 0.7 and –6.1 ± 0.8 V/s, respectively (n = 5) (Fig. 2*D*).

To facilitate the detection of any influence of glucose on electrical activity, the effects of the sugar were investigated in cells in which the action potential frequency was increased

by current injection (≤2 pA of current). In 4 different cells, the action potentials observed under these experimental conditions originated at –40 ± 3 mV, peaked at –9 ± 1 mV, and had a duration of 53 ± 2 ms. The amplitude of the action potential (determined as the difference between the peak of the action potential relative to the most negative interspike voltage) was 31 ± 2 mV, and the maximal upstroke and downstroke velocities were 1.7 ± 0.1 and –2.0 ± 0.1 V/s, respectively. It can be seen that increasing glucose to 20 mmol/l resulted in membrane repolarization from –44 ± 2 to –69 ± 2 mV (n = 6) and in the suppression of action potential firing (Fig. 2*A*). The observed glucose dependence of the electrical activity is precisely the opposite of that in the β-cell (20).

In insulin-secreting β-cells, electrical activity is tightly regulated by K_{ATP} channel activity (21). Therefore, we also tested for the presence of this channel in α-cells (Fig. 2*D*). In the presence of 3 mmol/l glucose, the K^+-dependent whole-cell conductance (G) averaged 90 ± 26 pS (n = 4). The conductance increased only marginally when the glucose concentration was raised to 20 mmol/l (i.e., when glucagon secretion and α-cell electrical activity are suppressed) and then amounted to 114 ± 23 nS (n = 4, data are not statistically different from those observed at 3 mmol/l), which is equivalent to an input resistance of 8.8 GΩ.

Addition of the K_{ATP} channel–opener diazoxide (200 µmol/l) increased the conductance 3-fold (300 ± 30%, n = 4, P < 0.01); this effect could be blocked with the addition of tolbutamide (200 µmol/l). This result suggests that mouse α-cells maintained in tissue culture contain a small number of K_{ATP} channels. Whole-cell infusion experiments confirm this conclusion. At low intracellular ATP levels (0.3 mmol/l), the whole-cell conductance averaged 276 ± 94 pS (n = 3), which was reduced to 140 ± 21 pS (n = 3) when ATP was included at a high (5 mmol/l) concentration in the pipette solution. It is worth pointing out that the magnitude of the whole-cell K_{ATP} conductance in the α-cell is small compared with that observed in mouse β-cells (10 nS) (20) and rat α-cells (20 nS) (11). The single-channel conductance (γ) of the K_{ATP} channel has been reported to be 19 pS with the intracellular solutions used in these experiments (22). In pancreatic β-cells, the open probability (P_{open}) of the K_{ATP} channels at 0.3 mmol/l intracellular ATP has been estimated as 0.11 ± 0.04 (S.B., unpublished data). The whole-cell conductance is given by the relationship $G = \gamma \cdot n \cdot P_{open}$ where n is the number of K_{ATP} channels per cell. If we assume the same value for P_{open} in α-cells as in β-cells, the observed whole-cell conductance in cells dialysed with 0.3 mmol/l ATP corresponds to fewer than 150 K_{ATP} channels per α-cell. The corresponding value in mouse β-cells is 7,000 ± 2,400 (n = 8) K_{ATP} channels (S.B., unpublished data).

Na^+ currents in the α-cells. To establish the mechanism responsible for the generation of action potentials in α-cells, we next investigated the voltage-gated currents using voltage-clamp protocols and the standard whole-cell configuration. When outward K^+ currents were suppressed by replacement of intracellular K^+ by Cs^+ and by adding extracellular TEA^+ (20 mmol/l), the inward currents responsible for the upstroke of the action potential could be discerned (Fig. 3*A*). These currents consisted of rapidly activating and inactivating currents as well as a more sustained component. The rapidly activating and inactivating component was blocked with TTX (Fig. 3*B*–*D*) and was activated at membrane potentials more positive than –30 mV. It peaked at +10 mV (Fig. 3*D*) and reached a maximal peak current amplitude of –200 ± 37 pA (n = 7). The activation can be described by the equation

$$I = G \cdot \frac{(V_m - V_r)}{1 + e^{\frac{-(V_m - V_h)}{k}}} \quad (4)$$

where I is the peak current, G is the whole-cell conductance (3.6 ± 0.4 nS), V_m is the voltage of the depolarizing pulse, V_r is the extrapolated reversal potential (70 ± 4 mV), V_h is the membrane potential at which the activation is half maximal, and k is the slope coefficient. Approximating the data points of 7 experiments to Eq. 4 gave values of V_h and k of –6 ± 2 and 7 ± 1 mV, respectively.

The Na^+ current characteristically underwent inactivation during depolarization. The steady-state inactivation properties of the current were studied using a conventional 2-pulse protocol in which a 5-ms test depolarization to zero was preceded by a 50-ms conditioning pulse to voltages between –100 and –10 mV (Fig. 3*E*). The equation

$$h_\infty = \frac{(1 - h_s)}{\left(1 + e^{\frac{-(V_h - V_m)}{k}}\right)} + h_s \quad (5)$$

was approximated to the normalized amplitude of the current h_∞ (the response after a conditioning pulse to –100 mV as unity). Here, V_m is the voltage during the conditioning pulse, h is the saturated level of h_∞, V_h is the membrane potential at which h_∞ is half-maximal, and k is the slope factor. In a series of 8 experiments, the values of V_h and k were determined as –42 ± 2 and –9 ± 2 mV (Fig. 3*F*). The value of h was 0.28 ± 0.04 (Fig. 3*F*), suggesting that close to one-third of the inward current flows through channels that do not inactivate during 50 ms. The noninactivating current exhibited characteristics similar to the TTX-resistant component (Fig. 3*B* and *E*). As illustrated in Fig. 4, this component is attributable to Ca^{2+} influx through voltage-gated Ca^{2+} channels.

Pharmacological and electrophysiological characteristics of the Ca^{2+} currents. The maximal peak amplitude for the remaining Ca^{2+} current determined in presence of TTX was –28 ± 4 pA (n = 7) during depolarizations to 10 mV and with 2.5 mmol/l Ca^{2+} as the charge carrier (Fig. 3*D*). When Ca^{2+} was replaced with 10 mmol/l Ba^{2+}, the peak current was maximal at zero and reached a peak amplitude of 59 ± 3 pA (n = 5) (Fig. 4*B*). The activation of the current could be approximated by a single exponential with a time constant of 2.2 ± 0.2 ms (n = 38) during a depolarization from –70 to 0 mV. Tail-current analysis was used to derive the activation properties of the Ca^{2+} current (Fig. 4*C*). The instantaneous tail current observed when stepping back to the holding potential (–70 mV) provides a measure of the number of Ca^{2+} channels that were activated during the preceding 5-ms depolarizing pulse. Fig. 4*D* summarizes the relationship between the voltage during the test pulse (V_m) and the amplitude of the subsequent tail current. The values of V_h and k (as previously defined) were –8 ± 2 and 8 ± 1 mV, respectively (n = 9) (Fig. 4*C* and *D*). Inactivation of Ba^{2+} currents flowing through the Ca^{2+}-channels was negligible during ≤50 ms depolarization (Fig. 4*A* and *C*).

It was recently demonstrated that both L- and N-type Ca^{2+} channels are present in α-cells obtained by fluorescence-activated cell sorting (5). There is also evidence of T-type currents in guinea pig α-cells (23). Here we have used the Ca^{2+} channel blockers nifedipine and ω-conotoxin to estimate the contribution of L- and N-type Ca^{2+} channels to the whole-cell Ca^{2+} current in mouse α-cells (Fig. 4*E* and *F*). The Ba^{2+} current flowing through the Ca^{2+} channels was partly (23 ± 4%) (n = 7) blocked by the N-type Ca^{2+} channel blocker ω-conotoxin. A further 46 ± 2% (n = 4) reduction of the control current amplitude was inhibited by application of the L-type Ca^{2+} channel blocker nifidepine (25 µmol/l). Finally, we tested the effects of Cd^{2+} (200 µmol/l, n = 9). This broad-spectrum Ca^{2+} channel blocker completely inhibited the remaining current, indicating that the α-cell, in addition to having nifedipine- and ω-conotoxin GVIA-sensitive Ca^{2+}-channels, is equipped with a third type of Ca^{2+} channel resistant to these Ca^{2+} channel blockers.

Delayed outward K^+ currents in the α-cell. We next investigated the voltage-gated K^+ conductances in the α-cell responsible for the repolarizing phase of the action potential. Outward currents evoked by a depolarization to 50 mV had a large outward component that averaged 664 ± 67 pA (n = 5). Figure 5*B* summarizes the current (I)-voltage (V) relationship of the K^+ current. The current activates at voltages beyond –20 mV and then increases with the applied voltage. The activation parameters were derived from the peak current amplitudes and the Eq. 4 yielding values of V_h and k of 9 ± 2 and 12 ± 1 mV, respectively (n = 6). The current was sensitive to TEA^+ (10 mmol/l), which reduced the outward component by 90 ± 1% (n = 5) (Fig. 5*A*).

Ca^{2+}-induced exocytosis in α-cells. Regulated exocytosis in neurons and many endocrine cells is triggered by influx of Ca^{2+} (24). We monitored exocytosis as increases in whole-cell capacitance, and we controlled $[Ca^{2+}]_i$ either by infusion of a Ca^{2+}/EGTA buffer through the recording electrode or by voltage-clamp depolarizations to open Ca^{2+} channels. When α-cells were infused with a solution containing 1.5 µmol/l $[Ca^{2+}]_i$, the whole-cell capacitance increased by 6.5 ± 0.9 pF (n = 7) during 222 ± 48 s (n = 7). During the linear increase in membrane capacitance (Fig. 6*A*), the rate of exocytosis was 42 ± 3 fF/s (n = 7). The latter value is much higher than the rate of capacitance increase measured from β-cells in the same preparation (identified by the larger cell capacitance and absence of Na^+ current), which averaged 8 ± 2 fF/s (n = 9). Measured cell capacitance did not change in α-cells infused with a Ca^{2+}-free solution, and the rate of capacitance increase was 1.0 ± 0.3 fF/s (n = 13).

We next investigated exocytosis elicited by voltage-clamp depolarizations. Varying the length of the depolarization from 5 to 850 ms (Fig. 6*B*) resulted in progressively larger capacitance increases. The relationship between pulse duration and the increase in cell capacitance (ΔC_m) in 8 different experiments is summarized in Fig. 6*C*. Capacitance increases of 50 ± 15 fF were observed already for pulse lengths as short as 30 ms; shorter pulses evoked measurable exocytotic responses in 50% of the cells tested. The relationship between pulse length and exocytotic response was clearly biphasic, consisting of an early component (lasting <300 ms) and a slower sustained phase.

Ca^{2+}-dependent exocytosis can be functionally divided into the release of granules from an IRP and the subsequent refilling of the IRP from a readily releasable pool (RRP) and a reserve pool (25). In chromaffine cells, the depletion of the IRP can be described by an exponential function (26). We hypothesize that this also applies to mouse pancreatic α-cells and that secretion reflects the sequential release of 2 pools of secretory granules according to the reaction scheme

$$RRP \underset{k_{-1}}{\overset{k_1}{\rightleftarrows}} IRP \xrightarrow{v_{exo}(t)} exocytosis \qquad (6)$$

Only granules that have proceeded into IRP are capable of undergoing exocytosis. The supply of granules into IRP from RRP is described by the rate constant k_1, and the reversal of the process is governed by the rate constant k_{-1}. Exocytosis proceeds at the speed $v_{exo}(t)$, which varies as a function of time. According to this model, the exchange of granules between RRP and IRP and the release can be described by the equation

$$\frac{dP_2}{dt} = -k_{-1} \cdot P_2 - v_{exo} \cdot P_2 + k_1 \qquad (7)$$

where P_2 is the variable size of the IRP.

To take into account the local differences in $[Ca^{2+}]_i$ and thus in the rate of exocytosis during the first milliseconds of the depolarization, v_{exo} is approximated by a sigmoidal function

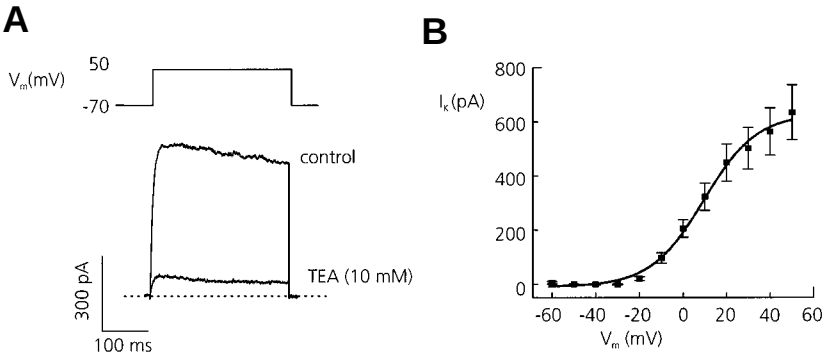

FIG. 5. Voltage-dependent K^+ conductance in the α-cell. *A*: Outward K^+ currents in response to voltage-clamp depolarizations to +50 mV before and after addition of 10 mmol/l TEA to the extracellular buffer. *B*: The *I-V* relationship of the delayed outward K^+ current evoked by 400-ms depolarizations to membrane potentials between –60 and +60 mV. The curve is drawn according to Eq. 4.

$$v_{exo} + \alpha_0 \cdot (1 - e^{-1/\tau}) \quad (8)$$

where α_0 is the rate constant of exocytosis from the IRP and τ is the time constant for the sigmoidal part that describes the rate of exocytosis for the short (≤30 ms) pulses. Inserting this expression into Eq. 7 yields

$$\frac{dP_2}{dt} = -k_{-1} \cdot P_2 - \alpha_0 \cdot (1 - e^{-t/\tau}) \cdot P_2 + k_1 \quad (9)$$

The size of the IRP, the rate constants k_1 and k_{-1}, α_0 and τ were determined by fitting Eq. 9 to the experimental data of capacitance measurements in Fig. 6*C*. In a series of 8 experiments, the size of the IRP was 158 ± 27 fF. The average values for k_1 and k_{-1}, α_0 and τ, were 409 ± 105, 0.095 ± 0.009 fF/s, 15 ± 3.6 s^{-1}, and 5.7 ± 0.8 ms. From the rate constant of exocytosis α_0, the value of τ_0 (the time constant for release of IRP) can be estimated (i.e., $ln2/\alpha_0$) to be 63 ± 13 ms. The time derivative of Eq. 9 for these values, shown in the inset of Fig. 6*C*, reveals that the speed of exocytosis is attained 21 ms after the onset of the depolarizing pulse. We estimated how Ca^{2+} influx through the Ca^{2+} channels varied during the action potential (see RESEARCH DESIGN AND METHODS, Eq. 1–3). This analysis revealed that 90% of the Ca^{2+} influx occurs during 22 ms (Fig. 6*D*). This result is close to the time needed to reach the maximal rate of exocytosis (Fig. 6*C*).

Mobilization of granules from reserve pool. The model previously described assumes that RRP is unlimited. This may be true in a mathematical sense, but it is obviously not the case in reality and, in the long run, exocytosis of granules belonging to IRP and RRP must be balanced by mobilization of new granules from the reserve pool. This becomes apparent during intense and repetitive stimulation of exocytosis as shown in Fig. 7. Here a train of ten 500-ms depolarizations to 0 mV (Fig. 7*A*) was applied to deplete RRP and IRP. The first depolarization evoked a large increase in cell capacitance (146 ± 54 fF, n = 14), whereas the total capacitance increase during the subsequent 4 depolarizations was small and

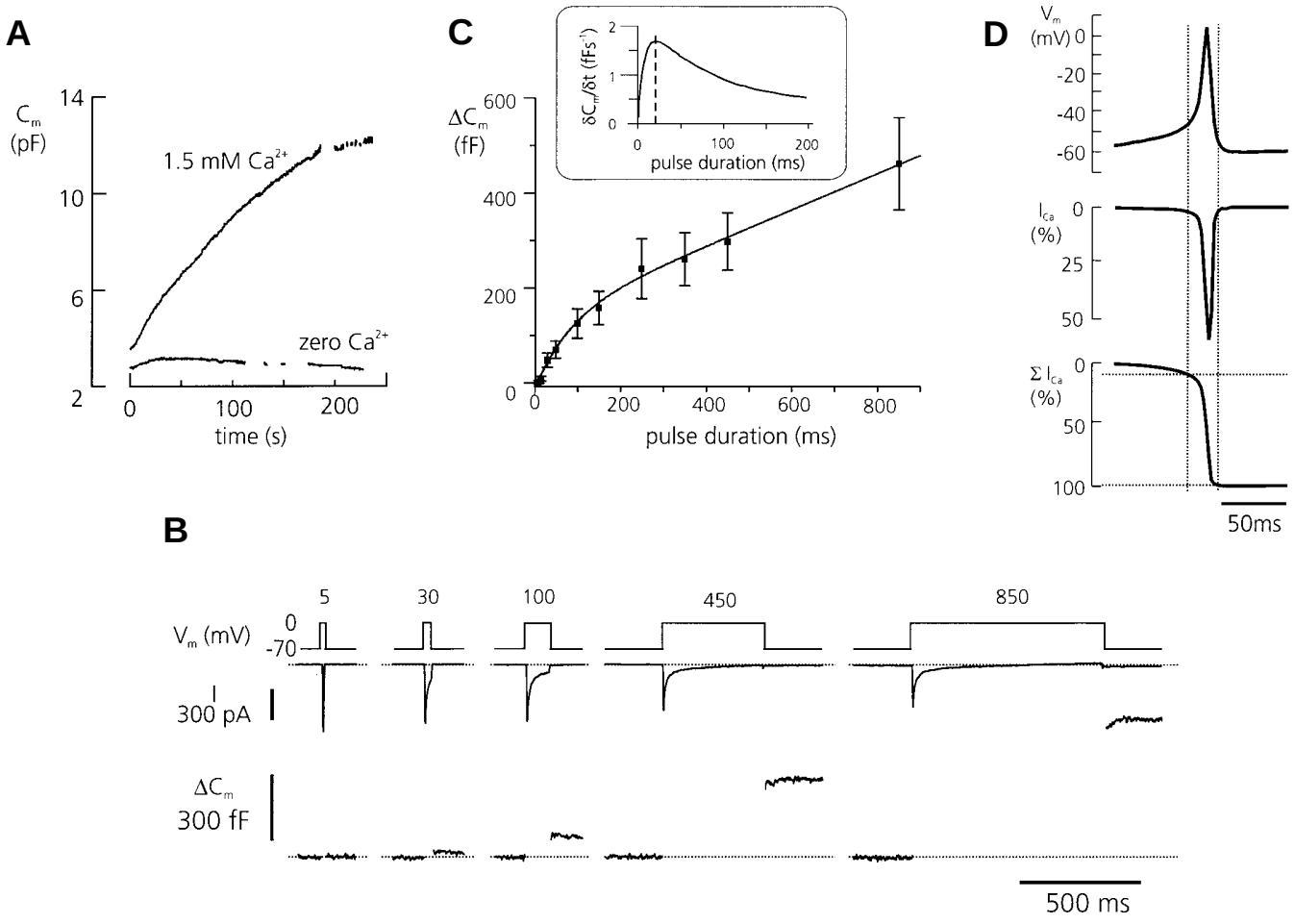

FIG. 6. Exocytosis from α-cells can be divided into the release from different functional pools. *A*: The capacitance increase upon infusion of Ca^{2+}/EGTA buffers with either 1.5 or 0 µmol/l $[Ca^{2+}]_i$. The rate of capacitance increase was 50 and 1.5 fF/s, respectively. *B*: Exocytosis (bottom trace) was elicited by voltage-clamp depolarizations from –70 to 0 mV lasting 5–850 ms (top trace). The inward currents elicited by the depolarizations are shown in the middle trace. Note that TTX is not present. *C*: The capacitance increase (ΔC_m) is plotted against the pulse duration. Data are the means ± SE of 8 experiments. The curve was drawn according to Eq. 9. *C* (inset): The derivative ($\delta C_m(t)/\delta t$) of the solution to Eq. 9. *D*: The average shape (n = 11) of the action potential (top tier) was combined with the activation properties (V_h, k, and τ) of the Ca^{2+} current to view the Ca^{2+} influx during the action potential (middle tier). The integral of the Ca^{2+} influx (bottom tier) during the action potential revealed that 90% of the Ca^{2+} influx occurs during 22 ms, as indicated by the dotted lines.

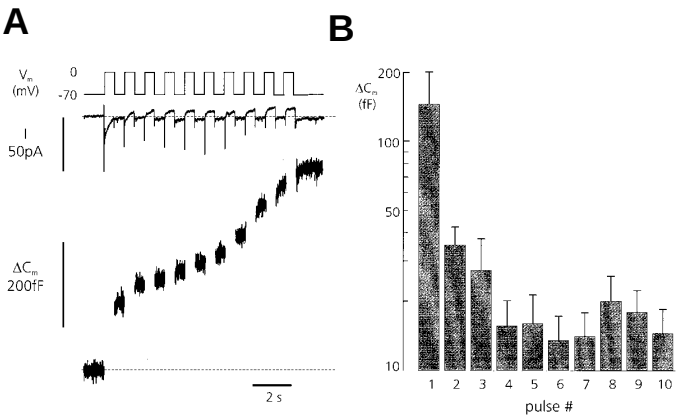

FIG. 7. Exocytosis during repetitive stimulation. *A*: The α-cell was stimulated by a train consisting of ten 500-ms depolarizations from –70 to 0 mV applied at 1 Hz (top). The evoked Ca^{2+} currents (*I*) (middle) and the associated increases in cell capacitance (ΔC_m) are shown. Note the presence of rapidly inactivating Na^+ currents. The total capacitance increase was 465 fF in this particular cell, of which 150 and 84 fF occurred during the first and 2–5 pulses, respectively. *B*: Histogram of the mean increase in cell capacitance (ΔC_m) displayed against the pulse number. Data are the means ± SE of the experiment in panel *A* and another 13 experiments of the same type.

totaled 95 ± 17 fF (n = 14). A secondary acceleration of exocytosis was observed after the sixth depolarization, and the capacitance increase during the entire train was 340 ± 73 fF. The rate of release during and between the last 4 depolarizations was 21 ± 5 fF/s, which is in the same range as the rate elicited by infusing the cell with 1.5 µmol/l free Ca^{2+} (as compared with that shown in Fig. 6*A*).

Determination of the α-cell granule diameter and number. Figure 8*A* shows an electron micrograph of a single α-cell in an islet. The electron-dense glucagon-containing granules differ from those of the β-cell by not showing a "halo." Several electron micrographs were used to determine the average diameter of the secretory granules within the α-cells. From the distribution of the apparent granule diameter of secretory granules (Fig. 8*B*), the true granule diameter was determined as 0.274 ± 0.014 µm (n = 768). The total number of granules was then estimated by multiplying the density (9.3 granules/µm^3) by the average volume of the α-cells (790 µm^3). A value of 7,320 ± 640 (n = 16 cells) was thus obtained.

DISCUSSION

α-Cells can be identified and studied in a standard mouse islet preparation. This study is based on the high fraction of α-cells in some cell preparations of mouse pancreatic islets. Although the islets that were used to prepare the cell cultures in this study contained only ~≤15% α-cells and >80% β-cells, the fraction of surviving β-cells in the preparation of dispersed cells ranged between 1 and 90%. The reason for the vulnerability of the β-cells in some preparations is not clear, and the mechanisms involved remain to be established. However, it is clear that the α-cells are more robust and tolerate the rough treatment required for the dissociation of the islets better than the β-cells.

We report that α-cells can be fairly easily and safely distinguished from β-cells during electrophysiological recordings by applying the following criteria: *1*) α-cells are significantly smaller than β-cells (3.7 vs. 6.2 pF); *2*) unlike the β-cells, the α-cells are electrically silent at high extracellular glucose levels; and *3*) the α-cells possess a large TTX-sensitive voltage-gated Na^+ current (100 pA), which, unlike its counterpart in β-cells, remains able to be activated at physiological membrane potentials (steady-state inactivation half-maximal at –42 mV). In retrospect, it seems possible that some published data, claimed to be obtained from β-cells, were in fact derived from α-cells, as the current records show signs of voltage-gated Na^+ currents (27).

Mouse α-cells are electrically excitable, and inhibition of electrical activity accounts for suppression of glucagon secretion. The stimulus-secretion coupling in the α-cells remains unclear. Rat pancreatic α-cells metabolize glucose,

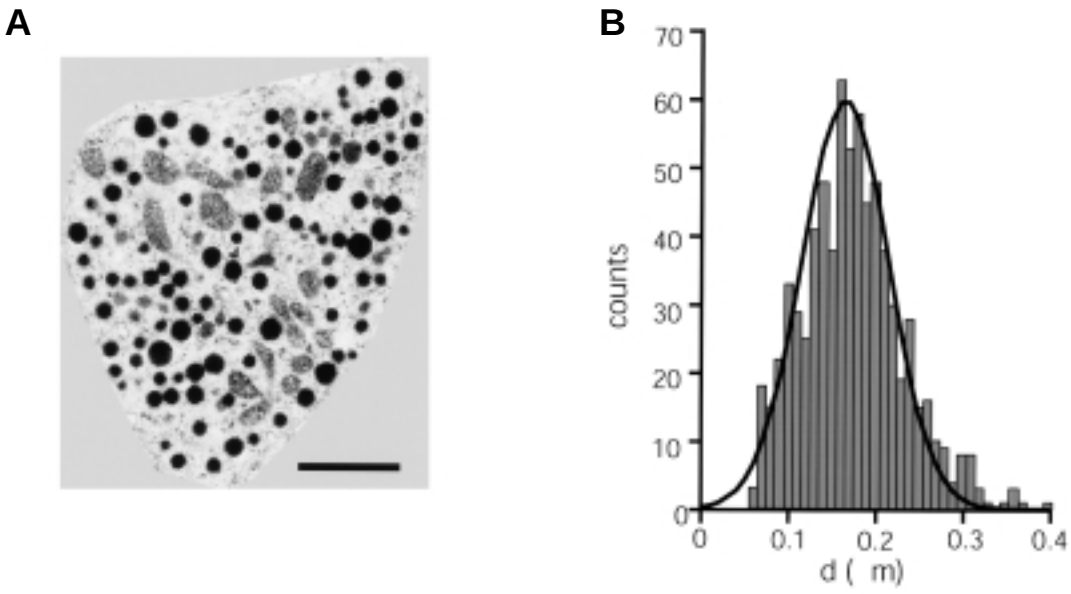

FIG. 8. Ultrastructure of the pancreatic α-cell. *A*: Electron micrograph of a mouse α-cell. Note the numerous electron-dense granules lacking a halo. The scale bar is 1 µm. *B*: Distribution of granule diameters. The continuous curve represents a Gaussian fit to the distribution, yielding a mean value of 274 ± 14 nm for the granule diameter.

albeit at a lower rate than β-cells, and the inhibitory action of the sugar on glucagon secretion is mediated by glucose metabolism (28). As previously documented for rat and guinea pig α-cells (5,9), mouse α-cells are electrically excitable and generate action potentials even in the absence of glucose. These action potentials reflect the activation of the voltage-gated Na^+ and Ca^{2+} channels during the upstroke of the action potential and of the voltage-gated K^+ channels during the repolarizing phase. The action potentials originate at membrane potentials as negative as –60 to –50 mV. The steady-state inactivation properties of the Na^+ channels are such that only ≥50% of the Na^+ current remains unable to be activated during the interspike period. The participation of the Na^+ channels in the depolarizing phase of the action potentials is suggested by the effects of moderate depolarization (up to –40 mV) evoked by current injection (Fig. 2*B–D*). This depolarization reduces the upstroke velocity (dV/dt_d) by >60%. This effect is likely attributable to the voltage-dependent inactivation of the Na^+ channels, which is half-maximal at –40 mV. The contribution of both Na^+ and Ca^{2+} channel to spike depolarization is suggested by comparison of the dV/dt_d and the peak inward current. The maximal value of dV/dt_d is observed about halfway through the upstroke (i.e., at –30 mV), at which it averaged 5 V/s. At –30 mV, the total inward current averaged ~20 pA. In a cell with a capacitance of ~4 pF, a current of this magnitude is sufficient to account for the observed value of dV/dt_d (5 V/s; note that $dV/dt_d = I/C$). Complete inactivation of the Na^+ current, as would be expected in Fig. 2*A*, reduces the inward current by two-thirds (Fig. 3*F*). The value of dV/dt_d can be expected to be reduced accordingly, and it averaged 1.7 V/s. The observed upstroke velocity (1.7 V/s) is in keeping with the contributions of the Na^+ channels to the action potential depolarization.

As expected for a glucagon-secreting cell, electrical activity was suppressed by an elevation of the glucose concentration from 3 to 20 mmol/l (Fig. 2*A*). We point out that this behavior is opposite to that of the β-cells, which start generating action potentials at glucose concentrations >5 mmol/l. Contrary to our expectations, we failed to observe any significant increase in membrane conductance when the glucose concentration was raised and the input resistance of the α-cell remained ~10 GΩ. Because the input resistance of the cell remains so high, even in the presence of glucose, a current of only a few picoamperes is sufficient to produce a repolarization of many millivolts (Fig. 2*B*). This finding may explain why arginine, which depolarizes the α-cell by its electrogenic entry, is a strong stimulus of glucagon secretion (9). Although the signaling pathways that underlie the glucose inhibitory action in the β-cell remain to be established, these early observations on isolated α-cells suggest that the ability of the sugar to reduce glucagon secretion does not solely (if at all) depend on paracrine mechanisms (10,13).

In keeping with previous observations in rat α-cells, mouse α-cells contain a tolbutamide- and diazoxide-sensitive membrane current, which is probably attributable to the activity of K_{ATP} channels, but the density of the channel is only 2% of that observed in mouse β-cells. The presence of K_{ATP} channels in α-cells is surprising, as their ATP-dependent closure (e.g., in response to glucose stimulation) would be expected to promote depolarization and stimulation of α-cell electrical activity. The role of K_{ATP} channels in the α-cell therefore remains mysterious.

Functional pools of secretory granules and different components of exocytosis. Varying the pulse duration between 5 and 850 ms allowed us to identify the size of the IRP to be 158 fF (Fig. 6*C*). The ultrastructural analysis indicates that the glucagon-containing secretory granules have a diameter of ~250 nm. Assuming spherical geometry and a specific membrane capacitance of 10 fF/μm^2 for the granular membrane, we estimate that a single granule in the α-cell contributes ~2 fF of capacitance upon fusion, which is similar to that in the β-cell (14). The size of the IRP is thus equivalent to 80 secretory granules or 1% of the total granule number (7,320 granules). The fraction of granules belonging to this pool is thus similar to that in insulin-secreting β-cells (29).

A striking difference between α- and β-cells is the behavior during a train of depolarizations. In the α-cells, a substantial fraction (51 ± 6%, n = 14) of the release occurs during the first pulse, whereas the subsequent 4–5 pulses evoke considerably smaller increases in cell capacitance. These data suggest that IRP and RRP are quickly depleted during secretion. In the β-cell, the decline between the first and second pulse is less pronounced (30). An interesting feature, which is also not observed in the β-cell, is the secondary acceleration seen at the end of the train. We interpret the slow component to reflect the mobilization of granules from the reserve pool. Therefore, it is worth noting that the rate of capacitance increase observed at the end of the train (20 fF/s) is comparable with the rate observed when the cell interior was dialyzed with an exocytotic concentration of $[Ca^{2+}]_i$ (42 fF/s).

Depolarizations as short as 30 ms consistently evoked exocytosis. This duration is close to that of the spontaneously generated α-cell action potential (31 ms), suggesting that individual action potentials are sufficient to trigger glucagon secretion. The speed of exocytosis reaches a maximum of 20 ms after the onset of the depolarization (Fig. 6*C*, inset). Interestingly, this value is the same as the duration of the period of Ca^{2+} entry during an action potential (Fig. 6*D*). This similarity means that the Ca^{2+} channels close exactly when the exocytotic rate starts to decline. Thus, it appears that the stimulus-secretion coupling in the α-cell is optimized for maximal utilization of Ca^{2+} entering through the Ca^{2+} channels for exocytosis.

The rate of exocytosis observed during infusion of the α-cells with 1.5 μmol/l $[Ca^{2+}]_i$ was much lower than that which could be elicited by voltage-clamp depolarizations (400–1,700 vs. 42 fF/s) (Fig. 6*A* and *C*), even when the measurements were carried out immediately after the establishment of the whole-cell configuration. This result is not unexpected given that exocytosis is initiated by depolarization too short to produce a uniform elevation of $[Ca^{2+}]_i$ within the cell, an observation suggesting that the Ca^{2+} channels and the secretory granules in the α-cell (as previously documented in β-cells [31]) colocalize so that secretion is determined by the $[Ca^{2+}]_i$ in the close vicinity of the Ca^{2+} channels (32). However, we emphasize that IRP and RRP are quickly depleted during the infusion experiments. Once these pools are emptied, the speed by which new granules are supplied for release (mobilization) becomes rate-limiting to exocytosis. If this hypothesis is correct, then the steady-state rate of capacitance increase should provide an estimate of the mobilization of granules from the reserve pool into the RRP. The observed rate of exocytosis in the infusion experiments (42 fF/s) thus corresponds to a supply rate of 21 granules/s using the conversion factor of 2 fF/gran-

ule. It is of interest that the rate of capacitance increase measured in the α-cells was 4-fold higher than that detected in β-cells of the same preparation. This indicates that the glucagon-secreting α-cell is equipped with a higher capacity for granule mobilization. In fact, comparing the size of IRP with the amplitude of total capacitance increase in the infusion experiments suggests that IRP turns over 34 times during the course of a 220-s experiment. The total increase in cell capacitance occurring during the infusion experiment (6.5 pF) corresponds to the discharge of 3,250 secretory granules. This value is equivalent to 44% of the total number of granules in the α-cell. It can be speculated that an efficient system for the refilling of the RRP in the α-cell represents a physiological adaptation reflecting the hyperglycemic action of glucagon and the importance of a continuous supply of glucose also during stress and starvation. It seems possible that, in the absence of mobilization, the IRP would quickly be depleted with resultant insufficient release of glucagon.

ACKNOWLEDGMENTS

We acknowledge the support of the Swedish Medical Research Council (Grants 8647 and 13147), the Swedish Diabetes Association, the Juvenile Diabetes Foundation International, the Novo Nordisk Foundation, the Knut och Alice Wallenbergs Stiftelse, the National Agency for Planning and Coordination of Research, the Crafoord Foundation, the Magnus Bergvalls Stiftelse, the Albert Påhlssons Stiftelse, and the Segerfalkska Stiftelsen.

We thank Kristina Borglid for excellent technical assistant.

REFERENCES

1. Unger RH, Orci L: Glucagon and the α-cell. *N Engl J Med* 304:1518–1524, 1575–1580, 1981
2. Gorus FK, Malaisse WJ, Pipeleers DG: Differences in glucose handling by pancreatic α- and β-cells. *J Biol Chem* 259:1196–1200, 1984
3. Pipeleers DG, Schuit FC, Van Schravendijk CFH, Van de Winkel M: Interplay of nutrients and hormones in the regulation of glucagon release. *Endocrinology* 117:817–823, 1985
4. Ding WG, Renström E, Rorsman P, Busschard K, Gromada J: Glucagon-like peptide I and glucose-dependent insulinotropic polypeptide stimulate Ca^{2+}-induced secretion in rat α-cells by a protein kinase A–mediated mechanism. *Diabetes* 46:792–800, 1997
5. Gromada J, Bokvist K, Ding WG, Barg S, Buschard, Renström E, Rorsman R: Adrenaline stimulates glucagon secretion in pancreatic α-cells by increasing the Ca^{2+} current and the number of granules close to the L-type Ca^{2+} channels. *J Gen Physiol* 110:217–228, 1997
6. Gerich JE, Charles MA, Grodsky GM: Regulation of pancreatic insulin and glucagon secretion. *Annu Rev Physiol* 38:353–388, 1976
7. Gromada J, Holst JJ, Rorsman P: Cellular regulation of islet hormone secretion by the incretin hormone glucagon-like peptide 1. *Pflügers Arch* 435:583–594, 1998.
8. Unger RH: Glucagon physiology and pathophysiology. *N Engl J Med* 19: 443–449, 1971
9. Rorsman P, Hellman B: Voltage-activated currents in guinea pig pancreatic α_2 cells: evidence for Ca^{2+}-dependent action potential. *J Gen Physiol* 91:223–242, 1988
10. Rorsman P, Berggren PO, Bokvist K, Ericson H, Möhler H, Östenson CG, Smith PA: Glucose-inhibition of glucagon secretion involves activation of $GABA_A$-receptor chloride channels. *Nature* 341:233–236, 1989
11. Bokvist K, Olsén HL, Hoy M, Gotfredsen CF, Holmes WF, Buschard K, Rorsman P, Gromada J: Characterisation of sulphonylurea and ATP-regulated K^+-channels in rat pancreatic α-cells. *Pflügers Arch* 438:428–436, 1999
12. Nadal A, Quesada I, Soria B: Homologous and heterologous asynchronicity between identified α-, β- and δ-cells within intact islets of Langerhans in the mouse. *J Physiol* 517:85–93, 1999
13. Berts A, Ball A, Gylfe E, Hellman B: Suppression of Ca^{2+} oscillations in glucagon-producing alpha 2-cells by insulin/glucose and amino acids. *Biochim Biophys Acta* 1310:212–216, 1996
14. Ämmälä C, Eliasson L, Bokvist K, Larsson O, Ashcroft FM, Rorsman P: Exocytosis elicited by action potentials and voltage-clamp calcium currents in individual mouse pancreatic β-cells. *J Physiol* 472:665–688, 1993
15. Martell AE, Smith RM (Eds.): *Critical Stability Constants*. Vols. 1 and 2. New York, Plenum Press, 1974
16. Rae J, Copper K, Gates P, Watsky M: Low access resistance perforated patch recordings using amphotericin B. *J Neurosci Methods* 37:15–26, 1991
17. Giger H, Riedwyl H: Bestimmung der Grossenverteilung von Kugeln aus Schnittkreisradien. *Biometr Zchr* 12:156–162, 1970
18. Dehoff RT, Rhines FN: Determination of the number of particles per unit volume from measurements made on random plane sections: the general cylinder and ellipsoid. *Trans Am Inst Mineral Met Engrs* 221:975–986, 1961
19. Göpel S, Kanno T, Barg S, Galvanovskis J, Rorsman P: Voltage-gated and resting membrane currents recorded from β-cells in intact mouse pancreatic islets. *J Physiol* 521:717–728, 1999
20. Rorsman P, Trube G: Glucose-dependent K^+-channels in pancreatic β-cells are regulated by intracellular ATP. *Pflügers Arch* 405:305–309, 1985
21. Rorsman P, Ashcroft FM: Electrophysiology of the pancreatic islet cells. *Progr Biophys Mol Biol* 54:87–143, 1989
22. Trube G, Rorsman P, Ohno-Shosaku T: Opposite effects of tolbutamide and diazoxide on the ATP-dependent K+ channel in pancreatic β-cells. *Pflügers Arch* 407:493–499, 1986
23. Rorsman P: Two types of Ca^{2+} currents with different sensitivity to organic Ca^{2+} channel antagonists in guinea pig pancreatic α_2 cells. *J Gen Physiol* 91:243–254, 1988
24. Burgoyne RD, Morgan A: Calcium sensors in regulated exocytosis. *Cell Calcium* 24:367–376, 1998
25. Neher E, Zucker RS: Multiple calcium-dependent processes related to secretion in bovine chromaffin cells. *Neuron* 10:21–30, 1993
26. Voets T, Neher E, Moser T: Mechanisms underlying phasic and sustained secretion in chromaffin cells from mouse adrenal slices. *Neuron* 23:607–615, 1999
27. Plant TD: Na^+ currents in cultured mouse pancreatic β-cells. *Pflügers Arch* 411:429–435, 1988
28. Heimberg H, De Vos A, Pipeleers D, Thorens B, Schuit F: Differences in glucose transporter gene expression between rat pancreatic α- and β-cells are correlated to differences in glucose transport but not in glucose utilization. *J Biol Chem* 270:8971–8975, 1995
29. Eliasson L, Renström E, Ding WG, Proks P, Rorsman P: Rapid ATP-dependent priming of secretory granules precedes Ca^{2+}-induced exocytosis in mouse pancreatic β-cells. *J Physiol* 503:399–412, 1997
30. Renström E, Eliasson L, Rorsman P: Protein kinase A-dependent and independent stimulation of exocytosis by cAMP in mouse pancreatic β-cells. *J Physiol* 502:105–118, 1997
31. Bokvist K, Eliasson L, Ämmälä C, Renström E, Rorsman P: Colocalization of L-type Ca^{2+} channels and insulin-containing secretory granules and its significance for the initiation of exocytosis in mouse pancreatic β-cells. *EMBO J* 14:50–57, 1995
32. Wiser O, Trus M, Hernández A, Renström E, Barg S, Rorsman P, Atlas D: The voltage sensitive Lc-type Ca^{2+} channel is functionally coupled to the exocytotic machinery. *Proc Natl Acad Sci U S A* 96:248–253, 1999